

Influence of mid-infrared Galactic bubble on surroundings: A case study on IRAS 16489-4431

Ariful HOQUE^{1,*}, Tapas BAUG^{1,*}, Lokesh DEWANGAN², Ke WANG³, Tie LIU⁴
and Soumen MONDAL¹

¹ S. N. Bose National Centre for Basic Sciences, Sector-III, Salt Lake, Kolkata-700 106, India

² Astronomy & Astrophysics Division, Physical Research Laboratory, Navrangpura, Ahmedabad 380009, India

³ Kavli Institute for Astronomy and Astrophysics, Peking University, Haidian District, Beijing 100871, People's Republic of China

⁴ Shanghai Astronomical Observatory, Chinese Academy of Sciences, 80 Nandan Road, Shanghai 200030, People's Republic of China

* Corresponding authors: ariful.hoque@bose.res.in, tapasbaug@bose.res.in

Abstract

We studied the influence of a massive star on a mid-infrared bubble and its surrounding gas in the IRAS 16489-4431 star-forming region using multi-wavelength data. The *Spitzer* mid-infrared band images revealed the shocked nature of the bubble. Analyses showed that the bubble is developed by a massive star owing to its strong radiation pressure. Evidence of collected material along the edge of the bubble was noted by the cold gas tracer line observed using Atacama Millimeter/submillimeter Array (ALMA). The presence of dense dust cores with bipolar outflows and young stellar objects toward the collected material is suggestive of active star formation possibly influenced by the expansion of the radiation driven bubble.

Keywords: Interstellar medium, Star formation, mid-infrared bubble, multi-wavelength

1. Introduction

Massive stars ($M_* > 8 M_\odot$), even though fewer in number, play a pivotal role in determining the evolution and ecology of their host galaxies (Zinnecker and Yorke, 2007). They, in general, affect their local environment throughout their life-time, by driving powerful jets and outflows, strong stellar winds, and by radiating substantial amounts of ultraviolet photons. Owing to such strong stellar feedback, they could either influence the surrounding gas for the formation of the next generation of stars or disperse the natal environment into the interstellar medium and halt further star formation (Deharveng et al., 2010).

Surrounding medium of a massive star gets ionized because of strong ultraviolet radiation, and develops an ionized region (i.e., HII region). Supersonic expansion of HII regions develop

shock fronts (Stromgren, 1939) and induce compression in neighboring molecular gas that morphologically appears as a bubble-like structure. Such bubbles were widely identified in *Spitzer* mid-infrared (MIR) $8\mu\text{m}$ band images (Churchwell et al., 2006, 2007).

Expansion of the MIR bubble could lead to the formation of new stars at the periphery of the bubbles (Deharveng et al., 2010; Dale et al., 2012). The compressed gas at the periphery of the bubbles may become gravitationally unstable and fragment into denser cores that can lead to the formation of stars (Elmegreen and Lada, 1977). Evidence of such star formation inferred by the presence of cluster of young stellar objects (YSOs), clumps and cores is found in several studies (see e.g., Baug et al. (2016, 2019); Dewangan et al. (2020); Das et al. (2017)).

In this paper, we study one such region, IRAS 16489-4431 where observations have shown the presence of a MIR bubble (Jayasinghe et al., 2019) and also cold mm-band cores around its periphery. The bubble was identified using a citizen science survey on the three-color images made using *Spitzer Space Telescope* Infrared Array Camera (IRAC; spatial resolution of $\sim 2''$) and Multiband Imaging Photometer for *Spitzer* (MIPS; spatial resolution $\sim 6''$) $24\mu\text{m}$ band images. The region is located at a near-kinematic distance of 3.26 kpc (Urquhart et al., 2018). A three color composite image of the region is shown in Fig. 1(a). Presence of an infrared dark cloud (IRDC) and pillars can be observed in the region. Presence of dust cores at the periphery of the bubble makes this region important for exploring the influence of a massive star on its surrounding gas. The paper is presented in the following manner. The data used in this paper are presented in Section 2. The results of this study are described in Section 3. A discussion of the results is presented in Section 4. Finally, we summarize the results in Section 5.

2. Data

ALMA data from ATOMS survey (Project ID: 2019.1.00685.S; PI: Tie Liu) are used in this study. The region was observed on 3 November 2019 with ALMA 12-m array in band 3. In this study, we used 3 mm continuum and H^{13}CO^+ data with a beam size of $\sim 2'' \times 2''$ having rms noise of 0.2 mJy beam^{-1} and 6.4 mJy beam^{-1} per 0.122 MHz channel, respectively. More details of the ALMA observations and data reduction can be found in Liu et al. (2020).

We have also utilized the archival survey data from Two Micron All Sky Survey (2MASS; Skrutskie et al., 2006), *Spitzer Space Telescope* Galactic Legacy Infrared Mid-Plane Survey Extraordinaire (GLIMPSE; Benjamin et al., 2003), Multiband Infrared Photometer for *Spitzer* (MIPS Carey et al., 2005), Wide-field Infrared Survey Explorer (WISE; Wright et al., 2010), and *Herschel* Photoconductor Array Camera and Spectrometer (PACS; Pilbratt et al., 2010).

3. Results

3.1. Cores: Identification and Mass Estimation

We identified the dust continuum cores in the ALMA 3 mm dust continuum image using the Python-based ASTRODENDRO package (Rosolowsky et al., 2008) that uses the dendrogram algorithm. We considered only those leaves (structures with no sub-structures) as cores that

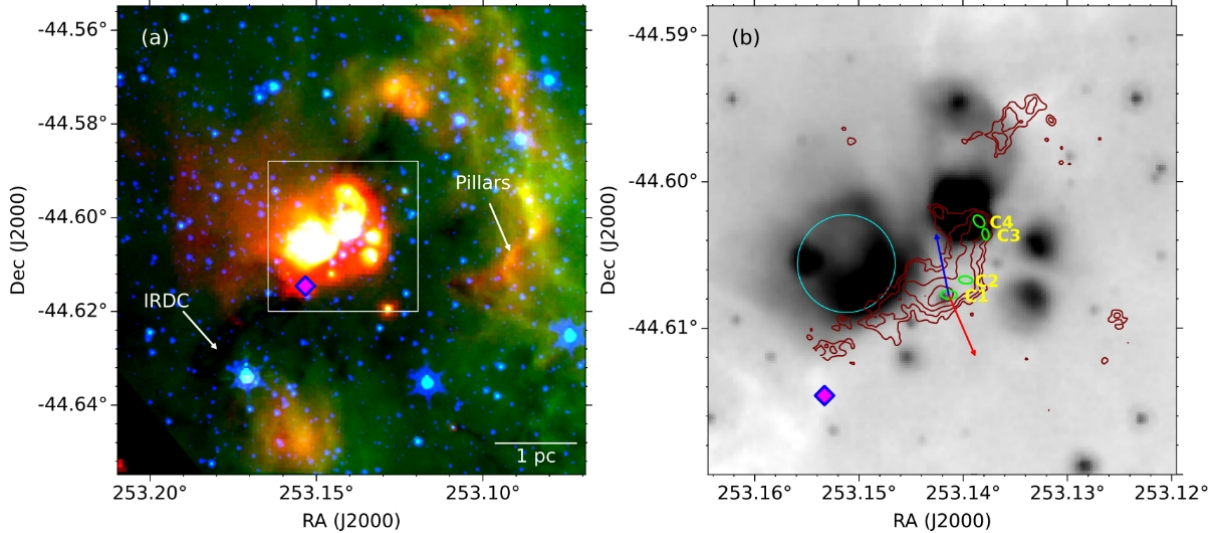


Figure 1: (a) A three-color composite image (red: $70 \mu\text{m}$, green: $8 \mu\text{m}$, and blue: $4.5 \mu\text{m}$) of the region. The white rectangle shows our target area for this study. A magenta diamond shows a Class II methanol maser source, and an IRDC and pillar-like structures are also labelled. (b) *Spitzer*-IRAC $8.0 \mu\text{m}$ image of target area overlaid with integrated H^{13}CO^+ contours in maroon drawn at $[3, 5, 8, 10] \times \sigma$ level. The cyan circle marks the MIR bubble. The cores are marked by ellipses and labelled (C1–C4). The red and blue arrows are the SiO outflow lobes associated with C1 (Baug et al., in prep).

have area more than 33 pixels (i.e., size of the beam in pixel) in ALMA 3 mm dust continuum image and have signal-to-noise ratio of more than 5. We identified four dust continuum cores (marked in Fig. 1(b)) and further refined their parameters using the CASA-IMFIT task (listed in Table 1).

With the assumption that dust emission is optically thin, the masses of the four identified cores are estimated using the equation from Hildebrand (1983),

$$M_{\text{core}} = \frac{F_{\nu} D^2 R_{\text{gd}}}{B_{\nu}(T_{\text{dust}}) \kappa_{\nu}} \quad (1)$$

where F_{ν} is integrated flux, D is distance to the region, R_{gd} is gas-to-dust ratio (adopted as 100), T_{dust} is dust temperature, $\kappa_{\nu} = 10(\nu/1.2 \text{ THz})^{\beta}$ is the dust opacity where β is the spectral index. For dust temperature, we examined the *Herschel* dust temperature map (Marsh et al., 2017). Fig. 2(a) shows the 3-mm ALMA dust continuum map of the region overlaid with *Herschel* dust temperature contours generated by Marsh et al. (2017) using a Point Process Mapping (PPMAP) algorithm on multi-band *Herschel* dust continuum images. The final resolution of the temperature map is $\sim 12''$. As can be seen in Fig. 2(a), all the identified dust continuum cores are located around T_{dust} contour of 21–22 K. Thus, we adapted an average T_{dust} of 21 K for all the cores. The mass of the cores were estimated for two β values of 1.5 and 2.0 and are listed in Table 1.

Table 1: Parameters of Identified Cores

Core [RA;Dec] (No [°;°])	Size	Int. Flux (mJy)	Peak Flux (mJy beam ⁻¹)	Mass (M _⊙) for T _{dust} = 21 K	
				β=1.5	β=2.0
C1 [253.1416;-44.6079]	2.0''×1.1''	2.7±0.1	1.4±0.1	9.9±0.2	34.3±0.8
C2 [253.1391;-44.6069]	1.7''×0.9''	2.1±0.1	1.3±0.1	7.8±0.3	27.1±1.0
C3 [253.1381;-44.6038]	1.4''×0.8''	13.2±0.9	8.7±0.4	48.3±2.2	167.4±7.5
C4 [253.1387;-44.6029]	2.6''×1.7''	6.0±0.1	2.1±0.1	21.8±0.3	75.7±0.9

3.2. Young Stellar Objects

We identified Young Stellar Objects (YSOs) using three different color-color and color-magnitude criteria, and then merged them together. We first applied [3.6]-[24]/[3.6] color criteria of Guieu et al. (2010) and Rebull et al. (2011) to identify young sources. Then, we utilize MIR ([5.8]-[8.0])/([3.6]-[4.5]) color criteria given in Gutermuth et al. (2009) to classify sources that are not detected or saturated in 24 μm images. There are also sources that are not detected in 8 μm band but detected in other IRAC bands, and for those we used ([3.6]-[4.5])/([4.5]-[5.8]) color-color scheme of Hartmann et al. (2005); Getman et al. (2007). For unified YSOs catalog, we finally performed a cross-matching of all the YSOs candidates, and removed the duplicacy (see Baug et al., 2016, for more details). We found a total of 8 Class I and 5 Class II sources within the targeted regions. The positions of the identified YSOs are marked in Fig. 2(b).

3.3. Shocked Bubble

IRAS 16489-4431 region contain a bubble at RA: 253.15107°, Dec: -44.60557° having an angular radius of 0.2' (Jayasinghe et al., 2019). Ratio map of *Spitzer*-IRAC images (e.g., Ch2/Ch1) can trace shocked regions as Ch2 includes shock excited H₂ emission and do not include any PAH features (Povich et al., 2007). Note that PAH emission can be triggered by both shock and ultra-violet radiation, but the H₂ line in Ch2 is solely shock excited. Thus, a bright extended emission in the ratio map can be inferred as a clear shocked region. On the otherhand, a dark extended emission in the ratio map is indicative of a tentative boundary of the shocked region. A clear shocked morphology can be noted in the ratio map shown in Fig. 2.

We searched for a possible influencing source of the bubble. Photometric search revealed one potential source (RA: 253.14996°, Dec: -44.60615°) with strong flux that could form the observed bubble. For confirmation, a fit to the observed fluxes (listed in Table 2) was performed using the SED-fitter tool of Robitaille et al. (2007). The input distance and interstellar visual extinction (A_V) ranges were set to 3.0-3.6 kpc and A_V ~3-30, respectively. Among the fitted models (see Fig. 3(a)), the models satisfying $\chi^2 - \chi_{\text{best}}^2 \leq 3$ were only considered in computing the mass of the source. The estimated mass of 7.9±0.7 M_⊙ is referring to a B2-B1 type star.

For a better knowledge of the feedback from the influencing star leading to the formation of the bubble, we computed different pressure components following the similar method outlined in Baug et al. (2019). The pressure due to radiation was estimated using, $P_{\text{rad}}=L_{\text{bol}}/4\pi cD_s^2$,

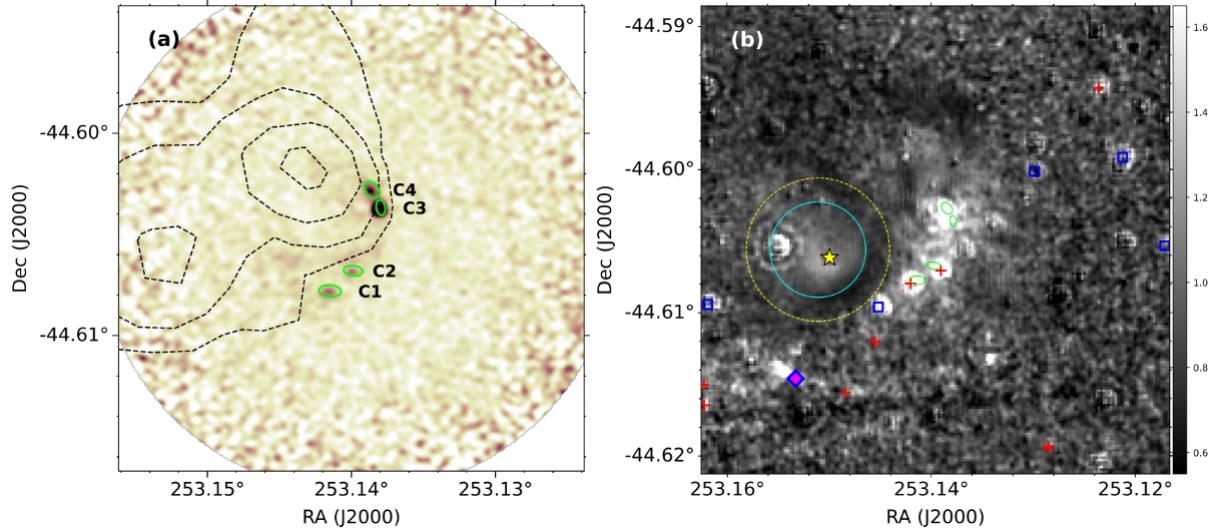


Figure 2: (a) ALMA 3 mm continuum map of IRAS 16489-4431 overlaid with *Herschel* dust temperature contours in black dashed lines drawn at 21, 22, 24 and 26 K. (b) Spitzer ratio map (Ch2/Ch1) of the target region. The position of Class I, Class II YSOs and the massive influencing star are marked by red pluses, blue squares and a yellow star, respectively. The yellow dashed circle shows a tentative outer (drawn by-eye) periphery of the shocked gas. The remaining symbols are the same as they are in Fig. 1.

Table 2: Photometric Magnitudes of the Influencing Source

J_{mag}	H_{mag}	K_{mag}	$W1_{\text{mag}}$	$W2_{\text{mag}}$	$W3_{\text{mag}}$	$W4_{\text{mag}}$
13.49 ± 0.04	12.27 ± 0.06	11.51 ± 0.05	7.58 ± 0.03	7.46 ± 0.02	3.32 ± 0.010	-0.160 ± 0.02

where L_{bol} is the bolometric luminosity of the star and D_s is the separation from the source. The pressure due to stellar wind was computed using, $P_w = \dot{M}V/4\pi D_s^2$, where \dot{M} is the mass-loss rate and V is the velocity of stellar wind. We did not compute the pressure for ionized gas as no radio continuum emission is detected within the bubble even in the recent CORNISH-South Survey (Irahor et al., 2023).

The pressure components as a function of separation from the driving source is shown in Fig. 3(b). We showed the P_{rad} for two masses, the lower limit of the fitted mass ($M \sim 7.2 M_{\odot}$) and $7.9 M_{\odot}$. The corresponding bolometric luminosities of 2690 and $3900 L_{\odot}$ are adopted from Lang (1999). For the calculation of P_w , $V \sim 700 \text{ km s}^{-1}$ and \dot{M} of $\sim 10^{-9.4} M_{\odot} \text{ yr}^{-1}$ for a typical B1V star were obtained from Oskinova et al. (2011). Fig. 3(b) shows that the radiation pressure dominates over stellar pressure and is sufficiently higher than the typical pressure exerted by cool giant molecular cloud ($\sim 10^{-12} - 10^{-11} \text{ dynes cm}^{-2}$ for a typical cloud temperature of 20 K and a particle density of $10^3 - 10^4 \text{ cm}^{-3}$; Dyson and Williams, 1980).

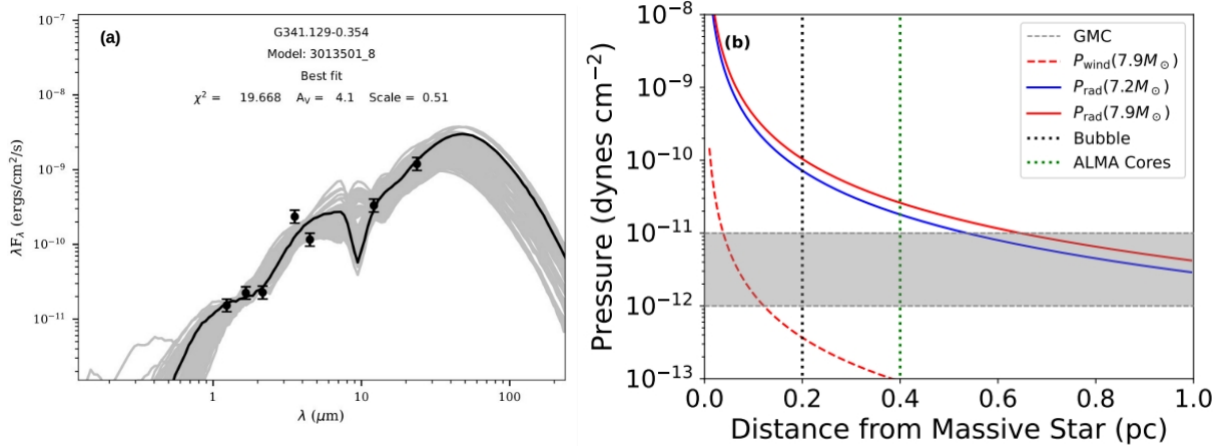


Figure 3: (a) SED fit to the fluxes (black dots; with typical 20% uncertainty) of the influencing source using the SED fitter tool of Robitaille et al. (2007). The solid black curve and gray curves are the best fit model and other good fits, respectively. (b) Plot of different pressure components exerted by the influencing star as a function of separation from the source. Radiation pressure for $7.9 M_{\odot}$ and $7.2 M_{\odot}$ stars are shown in red and blue solid curves. The wind pressure is shown in a red dashed curve. The gray area marks the pressure exerted by a typical cold giant molecular cloud with temperature of 20 K and a particle density of 10^3 – 10^4 cm^{-3} . The blue and green-dotted lines mark the average separation of the bubble edge and star-forming cores, respectively, from the influencing star.

4. Discussion

The primary aim of our study here is to assess the influence of a massive star on its surrounding gas. Jayasinghe et al. (2019) had reported the presence of a shocked-bubble in this region. Our analysis of IRAC-band images established the shocked nature of the bubble, and we also found that the bubble is developed by the strong radiation field driven by a massive $7.9 \pm 0.7 M_{\odot}$ star. In past decades, there have been several observational studies reported triggered star formation at the periphery of the MIR bubble (Povich et al., 2008; Smith et al., 2010; Yuan et al., 2014; Zhou et al., 2020).

Based on the smoothed particle hydrodynamic simulations of ionized-induced star formation in bound and unbound systems, Dale et al. (2012, 2013) argued that triggered star formation is most likely to occur at bubble edges or pillars, whereas spontaneous star formation could occur in both bubble edge and within the bubble cavity. Also in Dale et al. (2013) the authors suggested that the triggered stars formed at the bubble wall are younger than that are formed spontaneously and have strong accretion.

Our study shows the presence of collected materials (i.e., H^{13}CO^+ gas) towards the periphery of the bubble. Active star formation is also noted within the compressed material around the bubble inferred from the presence of YSOs and star-forming cores. In addition, one of the star-

forming cores is associated with bi-polar outflows, a typical signature for a young protostellar core. Presence of Class II methanol maser source toward the southern periphery of the bubble is indicative of active massive star formation. In brief, all the signatures in the IRAS 16489-4431 region hint toward an active star formation around the periphery of an expanding MIR bubble driven by a massive $7.9\pm 0.7 M_{\odot}$ star.

5. Summary

We performed a multiwavelength analysis of the local environment of the IRAS 16489-4431 region associated with a MIR bubble. Analysis of *Spitzer*-IRAC band images revealed shocked gas surrounding the edge of the bubble. We identified a possible massive $7.9\pm 0.7 M_{\odot}$ source which is driving the MIR bubble by its strong radiation pressure. ALMA cold gas tracer showed evidence of collected gas around the bubble periphery where all the dense cores are located. One of these cores is associated with bi-polar outflows indicative of active young star formation. The identified YSOs, specifically the Class I sources, are generally located around the edge of the shocked region. Overall, our analyses suggest that the radiation pressure from the $7.9\pm 0.7 M_{\odot}$ star has triggered the formation of the bubble and also might have influenced the star formation activity around the bubble periphery.

Acknowledgments

AH and TB thank the support by the S. N. Bose National Centre for Basic Sciences under the Department of Science and Technology, Govt. of India. AH also thanks the CSIR-HRDG for the funding of the Junior Research Fellow. This research makes use of astropy, a community-developed core python package for Astronomy (Astropy Collaboration, 2018). This paper makes use of the following ALMA data: ADS/JAO.ALMA 2019.1.00685.S and 2017.1.00545.S. ALMA is a partnership of ESO (representing its member states), NSF (USA), and NINS (Japan), together with NRC (Canada), MOST and ASIAA (Taiwan), and KASI (Republic of Korea), in cooperation with the Republic of Chile. The Joint ALMA Observatory is operated by ESO, AUI/NRAO, and NAOJ.

Further Information

ORCID identifiers of the authors

0009-0003-6633-525X (Ariful HOQUE)
0000-0003-0295-6586 (Tapas BAUG)
0000-0001-6725-0483 (Lokesh K. DEWANGAN)
0000-0002-7237-3856 (Ke WANG)
0000-0002-5286-2564 (Tie LIU)
0000-0003-1457-0541 (Soumen MONDAL)

Author contributions

All the authors of this paper have significantly contributed to the discussion and writing of this paper.

Conflicts of interest

The authors declare no conflict of interest.

References

- Astropy Collaboration (2018) The astropy project: Building an open-science project and status of the v2.0 core package. *AJ*, 156, 123. <https://doi.org/10.3847/1538-3881/aabc4f>.
- Baug, T., de Grijs, R., Dewangan, L. K., Herczeg, D. K., Gregory J. and Ojha, Wang, K., Deng, L. and Bhatt, B. C. (2019) Influence of wolf-rayet stars on surrounding star-forming molecular clouds. *ApJ*, 885(1), 68. <https://doi.org/10.3847/1538-4357/ab46be>.
- Baug, T., Dewangan, D. K., L. K. and Ojha and Ninan, J. P. (2016) Star formation around mid-infrared bubble n37: Evidence of cloud-cloud collision. *ApJ*, 833(1), 85. <https://doi.org/10.3847/1538-4357/833/1/85>.
- Benjamin, R. A., Churchwell, E., Babler, B. L., Bania, T. M., Clemens, D. P., Cohen, M., Dickey, J. M., Indebetouw, R., Jackson, J. M., Kobulnicky, H. A., Lazarian, A., Marston, A. P., Mathis, J. S., Meade, M. R., Seager, S., Stolovy, S. R., Watson, C., Whitney, B. A., Wolff, M. J. and Wolfire, M. G. (2003) Glimpse. i. an sirtf legacy project to map the inner galaxy. *MNRAS*, 115, 953–964. <https://doi.org/10.1086/376696>.
- Carey, S. J., Noriega-Crespo, A., Price, S. D., Padgett, D. L., Kraemer, K. E., Indebetouw, R., Mizuno, D. R., Ali, B., Berriman, G. B., Boulanger, F., Cutri, R. M., Ingalls, J. G., Kuchar, T. A., Latter, W. B., Marleau, F. R., Miville-Deschenes, M. A., Molinari, S., Rebull, L. M. and Testi, L. (2005) Mipsgal: A survey of the inner galactic plane at 24 and 70 microns, survey strategy and early results. *BAAS*, 37, 63.33.
- Churchwell, E., Povich, M. S., Allen, D., Taylor, M. G., Meade, M. R., Babler, B. L., Indebetouw, R., Watson, C., Whitney, B. A., Wolfire, M. G., Bania, T. M., Benjamin, R. A., Clemens, D. P., Cohen, M., Cyganowski, C. J., Jackson, J. M., Kobulnicky, H. A., Mathis, J. S., Mercer, E. P., Stolovy, S. R., Uzpen, B., Watson, D. F. and Wolff, M. J. (2006) The bubbling galactic disk. *ApJ*, 649(2), 759–778. <https://doi.org/10.1086/507015>.
- Churchwell, E., Watson, D. F., Povich, M. S., Taylor, M. G., Babler, B. L., Meade, M. R., Benjamin, R. A., Indebetouw, R. and Whitney, B. A. (2007) The bubbling galactic disk. ii. the inner 20°. *ApJ*, 670(1), 428–441. <https://doi.org/10.1086/521646>.
- Dale, J. E., Ercolano, B. and Bonnell, I. A. (2012) Ionization-induced star formation - IV. Triggering in bound clusters. *MNRAS*, 427(4), 2852–2865. <https://doi.org/10.1111/j.1365-2966.2012.22104.x>.

- Dale, J. E., Ercolano, B. and Bonnell, I. A. (2013) Ionization-induced star formation - V. Triggering in partially unbound clusters. *MNRAS*, 431(2), 1062–1076. <https://doi.org/10.1093/mnras/stt236>.
- Das, S. R., Tej, A., Vig, S., Liu, H.-L., Liu, T., Ishwara Chandra, C. H. and Ghosh, S. K. (2017) Infrared dust bubble cs51 and its interaction with the surrounding interstellar medium. *MNRAS*, 472(4), 4750–4768. <https://doi.org/10.1093/mnras/stx2290>.
- Deharveng, L., Schuller, F., Anderson, L. D., Zavagno, A., Wyrowski, F., Menten, K. M., Bronfman, L., Testi, L., Walmsley, C. M. and Wienen, M. (2010) A gallery of bubbles. the nature of the bubbles observed by spitzer and what atlasgal tells us about the surrounding neutral material. *A&A*, 523(A6). <https://doi.org/10.1051/0004-6361/201014422>.
- Dewangan, L. K., Baug, T., Pirogov, L. E. and Ojha, D. K. (2020) Investigating the physical conditions in extended system hosting mid-infrared bubble n14. *ApJ*, 898(1), 41. <https://doi.org/10.3847/1538-4357/ab964c>.
- Dyson, J. E. and Williams, D. A. (1980) *Physics of the interstellar medium*. Manchester: University Press.
- Elmegreen, B. G. and Lada, C. J. (1977) Sequential formation of subgroups in ob associations. *ApJ*, 214, 725–741. <https://doi.org/10.1086/155302>.
- Getman, K. V., Feigelson, E. D., Garmire, G., Broos, P. and Wang, J. (2007) X-ray study of triggered star formation and protostars in ic 1396n. *ApJ*, 654(1), 316–337. <https://doi.org/10.1086/509112>.
- Guieu, S., Rebull, L. M., Stauffer, J. R., Vrba, F. J., Noriega-Crespo, A., Spuck, T., Roelofsen Moody, T., Sepul, Cole, D. M., Flagey, N. and Laher, R. (2010) Spitzer observations of ic 2118. *ApJ*, 720(1), 46–63. <https://doi.org/10.1088/0004-637X/720/1/46>.
- Gutermuth, R. A., Megeath, S. T., Myers, P. C., Allen, L. E., Pipher, J. L. and Fazio, G. G. (2009) A spitzer survey of young stellar clusters within one kiloparsec of the sun: Cluster core extraction and basic structural analysis. *ApJS*, 184(1), 18–83. <https://doi.org/10.1088/0067-0049/184/1/18>.
- Hartmann, L., Megeath, S. T., Allen, L., Luhman, K., Calvet, N., D’Alessio, P., Franco-Hernandez, R. and Fazio, G. (2005) *Irac* observations of taurus pre-main-sequence stars. *ApJ*, 629(2), 881–896. <https://doi.org/10.1086/431472>.
- Hildebrand, R. H. (1983) The determination of cloud masses and dust characteristics from sub-millimetre thermal emission. *QJRAS*, 24(3), 267–282.
- Irabor, T., Hoare, M. G., Burton, M., Cotton, W. D., Diamond, P., Dougherty, S., Ellingsen, S. P., Fender, R., Fuller, G. A., Garrington, S., Goldsmith, P. F., Green, J., Gunn, A. G., Jackson, J., Kurtz, S., Lumsden, S. L., Marti, J., McDonald, I., Molinari, S., Moore, T. J., Mutale, M., Muxlow, T., O’Brien, T., Oudmaijer, R. D., Paladini, R., Pandian, J. D., Paredes,

- J. M., Richards, A. M. S., Sanchez-Monge, A., Spencer, R., Thompson, M. A., Umana, G., Urquhart, J. S., Wieringa, M. and Zijlstra, A. (2023) The coordinated radio and infrared survey for high-mass star formation - V. The CORNISH-South survey and catalogue. *MNRAS*, 520(1), 1073–1091. <https://doi.org/10.1093/mnras/stad005>.
- Jayasinghe, T., Dixon, D., Povich, M. S., Binder, B., Velasco, J., Lepore, D. M., Xu, D., Offner, S., Kobulnicky, H. A., Anderson, L. D., Kendrew, S. and Simpson, R. J. (2019) The milky way project second data release: bubbles and bow shocks. *MNRAS*, 488(1), 1141–1165. <https://doi.org/10.1093/mnras/stz1738>.
- Lang, K. R. (1999) *Astrophysical formulae*. New York : Springer.
- Liu, T., Evans, N. J., Kim, K., Goldsmith, P. F., Liu, S., Zhang, Q., Tatematsu, K., Wang, K., Juvela, M., Bronfman, L., Cunningham, M. R., Garay, G., Hirota, T., Lee, J., Kang, S., Li, D., Li, P., Mardones, D., Qin, S., Ristorcelli, I., Tej, A., Toth, L. V., Wu, J., Wu, Y., Yi, H., Yun, H., Liu, H., Peng, Y., Li, J., Li, S., Lee, C. W., Shen, Z., Baug, T., Wang, J., Zhang, Y., Issac, N., Zhu, F., Luo, Q., Soam, A., Liu, X., Xu, F., Wang, Y., Zhang, C., Ren, Z. and Zhang, C. (2020) Atoms: Alma three-millimeter observations of massive star-forming regions - i. survey description and a first look at g9.62+0.19. *MNRAS*, 496(3), 2790–2820. <https://doi.org/10.1093/mnras/staa1577>.
- Marsh, K. A., Whitworth, A. P., Lomax, O., Ragan, S. E., Becciani, U., Cambr esy, L., Di Giorgio, A., Eden, D., Elia, D., Kacsuk, P., Molinari, S., Palmeirim, P., Pezzuto, S., Schneider, N., Sciacca, E. and Vitello, F. (2017) Multitemperature mapping of dust structures throughout the Galactic Plane using the PPMAP tool with Herschel Hi-GAL data. *MNRAS*, 471(3), 2730–2742. <https://doi.org/10.1093/mnras/stx1723>.
- Oskinova, L. M., Todt, H., Ignace, R., Brown, J. C., Cassinelli, J. P. and Hamann, W. R. (2011) Early magnetic b-type stars: X-ray emission and wind properties. *MNRAS*, 416(2), 1456–1474. <https://doi.org/10.1111/j.1365-2966.2011.19143.x>.
- Pilbratt, G. L., Riedinger, J. R., Passvogel, T., Crone, G., Doyle, D., Gageur, U., Heras, A. M., Jewell, C., Metcalfe, L., Ott, S. and Schmidt, M. (2010) Herschel space observatory. an esa facility for far-infrared and submillimetre astronomy. *A&A*, 518, L1. <https://doi.org/10.1051/0004-6361/201014759>.
- Povich, M. S., Benjamin, R. A., Whitney, B. A., Babler, B. L., Indebetouw, R., Meade, M. R. and Churchwell, E. (2008) Interstellar weather vanes: Glimpse mid-infrared stellar wind bow shocks in m17 and rcw 49. *ApJ*, 689(1), 242–248. <https://doi.org/10.1086/431472>.
- Povich, M. S., Stone, J. M., Churchwell, E., Zweibel, E. G., Wolfire, M. G., Babler, B. L., Indebetouw, R., Meade, M. R. and Whitney, B. A. (2007) A multiwavelength study of m17: The spectral energy distribution and pah emission morphology of a massive star formation region. *ApJ*, 660(1), 346–362. <https://doi.org/10.1086/513073>.

- Rebull, L. M., Johnson, C. H., Hoette, V., Kim, J. S., Laine, S., Foster, M., Laher, R., Legassie, M., Mallory, C. R. and McCarron, K. (2011) New young star candidates in cg4 and sa101. *AJ*, 142(1), 25–46. <https://doi.org/10.1088/0004-6256/142/1/25>.
- Robitaille, T. P., Whitney, B. A., Indebetouw, R. and Wood, K. (2007) Interpreting spectral energy distributions from young stellar objects. ii. fitting observed seds using a large grid of precomputed models. *ApJS*, 169(2), 328–352. <https://doi.org/10.1086/512039>.
- Rosolowsky, E. W., Pineda, J. E., Kauffmann, J. and Goodman, A. A. (2008) Structural analysis of molecular clouds: Dendrograms. *ApJ*, 679(2), 1338–1351. <https://doi.org/10.1086/587685>.
- Skrutskie, M. F., Cutri, R. M., Stiening, R., Weinberg, M. D., Schneider, S., Carpenter, J. M., Beichman, C., Capps, R., Chester, T., Elias, J., Huchra, J., Liebert, J., Lonsdale, C., Monet, D. G., Price, S., Seitzer, P., Jarrett, T., Kirkpatrick, J. D., Gizis, J. E., Howard, E., Evans, T., Fowler, J., Fullmer, L., Hurt, R., Light, R., Kopan, E. L., Marsh, K. A., McCallon, H. L., Tam, R., Van Dyk, S. and Wheelock, S. (2006) The two micron all sky survey (2mass). *AJ*, 131(2), 1163–1183. <https://doi.org/10.1086/498708>.
- Smith, N., Povich, M. S., Whitney, B. A., Churchwell, E., Babler, B. L., Meade, M. R., Bally, J., Gehrz, R. D., Robitaille, T. P. and Stassun, K. G. (2010) Spitzer space telescope observations of the carina nebula: the steady march of feedback-driven star formation. *MNRAS*, 402(2), 952–974. <https://doi.org/10.1111/j.1365-2966.2010.16792.x>.
- Stromgren, B. (1939) The physical state of interstellar hydrogen. *ApJ*, 89, 526–547. <https://doi.org/10.1086/144074>.
- Urquhart, J. S., Konig, C., Giannetti, A., Leurini, S., Moore, T. J. T., Eden, D. J., Pillai, T., Thompson, M. A., Braiding, C., Burton, M. G., Csengeri, T., Dempsey, J. T., Figura, C., Froebrich, D., Menten, K. M., Schuller, F. and Smith, M. D., M. D. and Wyrowski (2018) Atlasgal-properties of a complete sample of galactic clumps. *MNRAS*, 473(1), 1059–1102. <https://doi.org/10.1093/mnras/stx2258>.
- Wright, E. L., Eisenhardt, P. R. M., Mainzer, A. K., Ressler, M. E., Cutri, R. M., Jarrett, T., Kirkpatrick, J. D., Padgett, D., McMillan, R. S., Skrutskie, M., Stanford, S. A., Cohen, M., Walker, R. G., Mather, J. C., Leisawitz, D., Gautier, T. N., McLean, I., Benford, D., Lonsdale, C. J., Blain, A., Mendez, B., Irace, W. R., Duval, V., Liu, F., Royer, D., Heinrichsen, I., Howard, J., Shannon, M., Kendall, M., Walsh, A. L., Larsen, M., Cardon, J. G., Schick, S., Schwalm, M., Abid, M., Fabinsky, B., Naes, L. and Tsai, C. (2010) The wide-field infrared survey explorer (wise): Mission description and initial on-orbit performance. *AJ*, 140(6), 1868–1881. <https://doi.org/10.1088/0004-6256/140/6/1868>.
- Yuan, J.-H., Wu, Y., Li, J. Z. and Liu, H. (2014) Expanding Shell and Star Formation in the Infrared Dust Bubble N6. *ApJ*, 797(1), 40. <https://doi.org/10.1088/0004-637X/797/1/40>.

Zhou, J., Zhou, D., Esimbek, J., Baan, W., Wu, G., Ji, W., He, Y., Li, D., Sailanbek, S., Komesh, T. and Tang, X. (2020) G15.684-0.29: One of the Largest Galactic Infrared Bubbles Showing Strong Evidence of Triggered Star Formation. *ApJ*, 897(1), 74. <https://doi.org/10.3847/1538-4357/ab94c0>.

Zinnecker, H. and Yorke, H. W. (2007) Toward understanding massive star formation. *ARA&A*, 45(1), 481–563. <https://doi.org/10.1146/annurev.astro.44.051905.092549>.